



HAL
open science

Exploring Fast Room Temperature Oxygen Diffusion in Pr₂NiO_{4+δ} Stand-Alone Single-Crystalline Electrodes

Avishek Maity, Rajesh Dutta, Oles Sendtskyi, Monica Ceretti, Angélique Lebranchu, Dmitry Chernyshov, Alexeï Bosak, Werner Paulus

► **To cite this version:**

Avishek Maity, Rajesh Dutta, Oles Sendtskyi, Monica Ceretti, Angélique Lebranchu, et al.. Exploring Fast Room Temperature Oxygen Diffusion in Pr₂NiO_{4+δ} Stand-Alone Single-Crystalline Electrodes. Chemistry of Materials, 2022, 34 (1), pp.414-421. 10.1021/acs.chemmater.1c03847 . hal-03523157

HAL Id: hal-03523157

<https://hal.science/hal-03523157>

Submitted on 12 Jan 2022

HAL is a multi-disciplinary open access archive for the deposit and dissemination of scientific research documents, whether they are published or not. The documents may come from teaching and research institutions in France or abroad, or from public or private research centers.

L'archive ouverte pluridisciplinaire **HAL**, est destinée au dépôt et à la diffusion de documents scientifiques de niveau recherche, publiés ou non, émanant des établissements d'enseignement et de recherche français ou étrangers, des laboratoires publics ou privés.

Exploring fast room temperature oxygen diffusion in $\text{Pr}_2\text{NiO}_{4+\delta}$ stand-alone single crystalline electrodes

Avishek Maity^{a,‡}, Rajesh Dutta^{a,‡}, Oles Sendtskyi^{a, &}, Monica Ceretti^a, Angélique Lebranchu^a, Dmitry Chernyshov^b, Alexei Bosak^c, Werner Paulus^{a}*

a ICGM, Université de Montpellier, CNRS, ENSCM, 34293 Montpellier, France.

b Swiss-Norwegian Beam Lines at European Synchrotron Radiation Facility, 71 avenue des Martyrs, 38043 Grenoble, France

c European Synchrotron Radiation Facility, 71 avenue des Martyrs, 38043 Grenoble, France

KEYWORDS: Pr_2NiO_4 , transition metal oxides, non-stoichiometric oxides, in situ diffraction, synchrotron diffraction, oxygen ion conductors, single crystal electrode, domain ordering, electrochemistry

ABSTRACT. Performant solid-state oxygen ion conductors are of utmost importance for current and future energy applications. A significant enhancement of oxygen mobility has been recently established in the intermediate temperature range from 500-700°C, but materials showing notable room temperature oxygen diffusion are still rare. Whereas devices for energy storage or

transformation generally employ polycrystalline electrodes, we report here on the electrochemical oxygen permeation capacity of single crystalline $\text{Pr}_2\text{NiO}_{4+\delta}$ electrodes, showing remarkably high oxygen diffusion at ambient conditions, whilst $60\ \mu\text{m}$ thick. The electrochemically performed oxygen reduction was followed up by in situ single crystal synchrotron diffraction, revealing oxygen mass transport corresponding to a chemical diffusion coefficient of $D^* = 6.3 \times 10^{-11}\ \text{cm}^2\text{s}^{-1}$. Rapid oxygen diffusion becomes possible due to the predominant absence of grain boundaries, as revealed from the evolution of the individual twin domains. For the first time, the formation of anti-phase domains, organized on a length scale of $7\ \text{nm}$, could be evidenced during a chemical reaction, indicated by sharp satellite reflections of 2nd order. Our results demonstrate the yet unexplored potential of single crystals as stand-alone electrodes for high-throughput solid oxygen ion conductors at already ambient conditions.

INTRODUCTION

Mixed ionic-electronic conductors are an important class of materials for a variety of technological applications such as energy conversion and storage devices, fuel-cells, supercapacitors, oxygen separation, catalysts and electrocatalyst.¹⁻⁴ Different strategies have been used to enhance oxygen ion conductivity at already moderate temperatures, but the role of pure bulk and interface oxygen diffusion is still not fully explored. The modification and engineering of grain boundaries in terms of stoichiometry, dislocations and specific microstructures has been recently investigated on thin films, indicating fast oxygen diffusion pathways around 500°C at the interface, which to a certain extent can be decoupled from the bulk diffusion.⁵⁻⁹ Thereby the increase of the oxygen mobility can attain several orders of magnitude, while the diffusion mechanism itself is far from being understood. On the other hand, low-T oxygen diffusion mechanisms have been reported to be phonon assisted and related to structural instabilities,

supported by DFT simulations down to ambient temperature for several non-stoichiometric Ruddlesden-Popper type oxides.¹⁰⁻¹⁶ $\text{Pr}_2\text{NiO}_{4+\delta}$ presents one of the most promising oxygen membranes already at moderate temperatures, for which oxygen diffusion pathways have been visualized from neutron scattering density maps for $\text{Pr}_2\text{NiO}_{4+\delta}$ single crystals, evidencing an almost continuous dynamically activated overlap between apical and interstitial lattice sites at 400°C.^{6, 10, 17-20} Further on electrochemical oxidation/reduction of polycrystalline $\text{Pr}_2\text{NiO}_{4+\delta}$ electrodes, carried out at room temperature (RT) in an aqueous alkaline solution, showed that oxygen ions can be intercalated reversibly, revealing a rich phase diagram.²¹

Moreover, spontaneous topotactic oxygen diffusion in $\text{Pr}_2\text{NiO}_{4+\delta}$ even at ambient temperature has been recently shown to be linked to sub-mesoscale oxygen ordering. Thereby, translational periodicities of more than 100 Å were uncovered, thus contradicting the paradigm that performant ionic conductivity is intrinsically related to structural disorder.²² In this work we were interested to deepen the structural insights of the oxygen diffusion mechanism of $\text{Pr}_2\text{NiO}_{4+\delta}$ by re-investigating the oxygen intercalation reaction by in situ single crystal synchrotron diffraction. 3D reciprocal lattice scanning allows to obtain valuable information as diffuse scattering, low intensity superstructure reflections, but also quantitative values of the volume fraction of twin domains and related microstructural changes during a chemical reaction, impossible to access with powder diffraction methods. We show in the following the necessity to use single crystalline electrodes to access all these details simultaneously by in situ diffraction studies under applied electrochemical potential.

On the other hand, we could evidence for the first time, anti-phase domain ordering with a periodicity of 7 nm, together with a significantly faster oxygen diffusion kinetics in single crystalline electrodes, related to the major absence of grain boundaries. It underlines together

with sub-mesoscopic oxygen ordering, the importance competitive, weak interactions may play, to trigger long-range ordering phenomena for diffusion processes at ambient conditions, and which are largely unexplored so far.

EXPERIMENTAL

Single crystal growth. Single crystals of $\text{Pr}_2\text{NiO}_{4.25}$ have been successfully grown by the floating zone method at ICGM as described in ref ²³, resulting in a diameter of about 6 mm while reaching lengths of more than 10 cm.²⁴

Synchrotron and X-ray diffraction experiments. Diffraction experiments have been carried out on BM01, SNBL@ESRF at $\lambda = 0.6630 \text{ \AA}$, using the 2M Pilatus detector. The electrochemical reduction of $\text{Pr}_2\text{NiO}_{4.225}$ was followed up by *in situ* single crystal synchrotron diffraction on a $60 \times 60 \times 1000 \mu\text{m}^3$ shaped crystal in a specifically adapted electrochemical set-up (see Fig S1). Size and shape of the crystal were chosen to optimize the reaction kinetics, and consequently to minimize any inhomogeneous phase formation during the discharge reaction. In this regard, the [001] longitudinal direction of the needle shaped crystal allows a maximized oxygen diffusion along the [110] direction inside the Pr_2O_3 rock salt layer, here presenting the shortest crystal dimension. The crystals was transferred into the electrochemical cell, consisting of two Debye-Scherrer quartz capillaries as described in ref ²⁵. In order to minimize absorption and extinction problems, the crystal was turned around its long axis (200° in steps of $0.1^\circ/\text{image}$), the exposure time being 0.5 s/frame, resulting in a collection time of about 17 min per dataset. The whole reaction was finished in 20 hours, thus yielding 72 complete data collections corresponding to a variation of $\Delta\delta = 0.003$ oxygen/f.u. per data set. With a linear absorption coefficient of 231cm^{-1} , the transmission for a $60 \mu\text{m}$ thick crystal amounts to at

minima to 25%, which is still a very satisfying value, guaranteeing to obtain a volume information throughout the crystal. The electrochemical reaction required to apply a permanent current of $10 \mu\text{A}$, to overcome problems related to parasitic currents as outlined in the text below. The applied reaction conditions consequently involve a continuous production of hydrogen bubbles at the crystal site inside the capillary, which perturbs the data analysis as it changes the total absorption behavior and changes locally the current density of the setup. This problem could be overcome by constantly pumping fresh 1N-KOH electrolyte through the inner capillary at a velocity of 5ml/min, and which evacuated all additionally generated hydrogen instantly.

Data Analysis. Single crystal data analysis has been performed using the SNBL Tool Box²⁶, the CrysAlis pro (Rigaku) and ALBULA software package (Dectris) as well as the X-Area software package (STOE Darmstadt).

RESULTS AND DISCUSSION

The structure of $\text{Pr}_2\text{NiO}_{4+\delta}$ is generally schematized as a layer structure consisting of corner shared NiO_6 octahedra where in between are inserted Pr atoms as spacers (Figure 1a). Oxygen diffusion has been shown to be highly anisotropic,^{16, 18, 20, 27} with a diffusion pathway involving a direct and dynamically activated exchange of oxygen atoms between apical and interstitial lattice sites inside the rock salt type Pr_2O_2 layers, as outlined in Fig 1b. Interstitial lattice sites can accommodate extra oxygen atoms, which are coordinated by 4 Pr and 4 O_{ap} atoms, both forming a tetrahedron. For $\text{Pr}_2\text{NiO}_{4.25}$ only one eighth of all available tetrahedral sites are occupied,

leaving most of these sites vacant, promoting oxygen diffusion via a kind of push-pull diffusion mechanism.

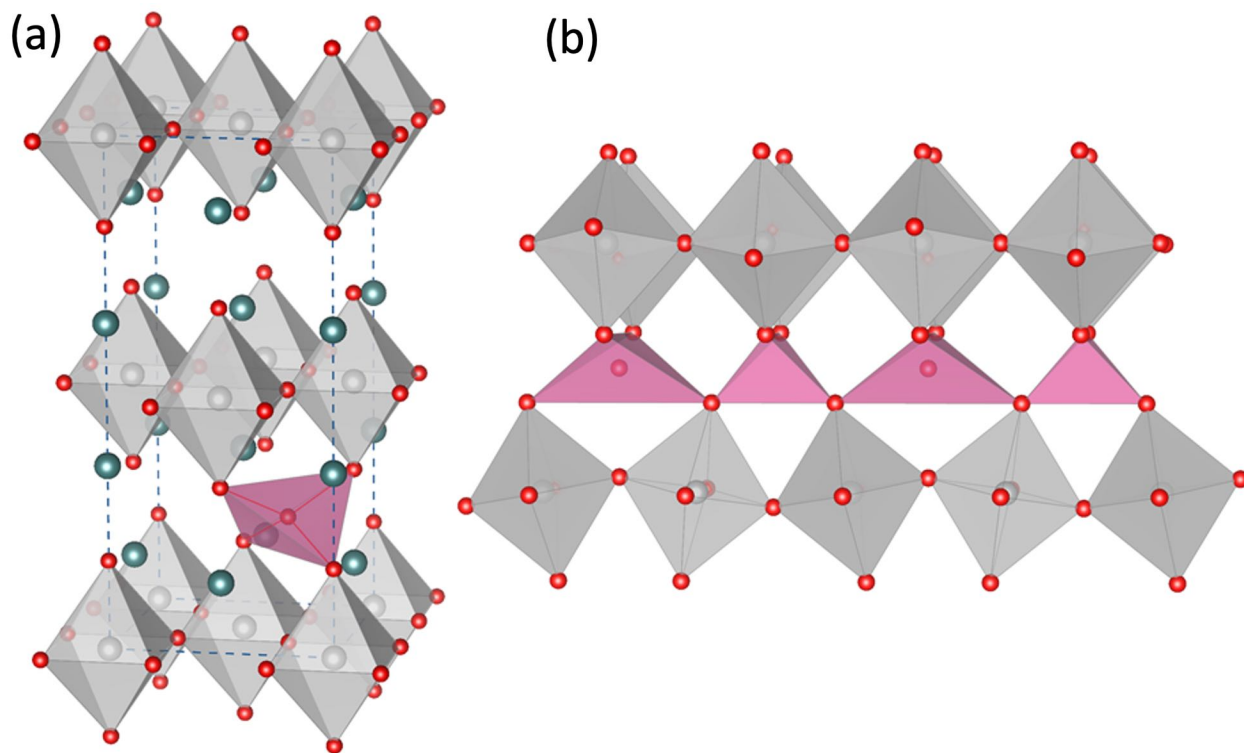


Figure 1: (a) idealized structure scheme of $\text{Pr}_2\text{NiO}_{4+\delta}$, one out of 8 possible interstitial oxygen sites is indicated, Pr: green, Ni: gray, O: red. (b): oxygen diffusion pathway inside the Pr_2O_2 layer, indicating the local deformations of the bigger $\text{O}_{\text{int}}(\text{O}_{\text{ap}})_4$ and smaller $\text{O}_{\text{vac}}(\text{O}_{\text{ap}})_4$ tetrahedra along the [110] diffusion pathway; in (b) Pr atoms are omitted for clarity.

For the electrochemically obtained phase diagram of $\text{Pr}_2\text{NiO}_{4+\delta}$, *in situ* neutron powder diffraction studies revealed three distinct phases.²¹ Two of them were identified as stoichiometric

line phases with orthorhombic symmetry, $\text{Pr}_2\text{NiO}_{4.225}$ and $\text{Pr}_2\text{NiO}_{4.00}$, the additional intermediate non-stoichiometric phase $\text{Pr}_2\text{NiO}_{4.08\pm 0.02}$ is tetragonal. The symmetry changes during the course of reduction pass from orthorhombic to tetragonal to become again orthorhombic for the fully reduced phase. The sequence of three phases may be considered as a “re-entrant” transition in the sense that the same translational symmetry reappears in the structure for the end members but differs from that for the intermediate phase.

Recently, the structure of $\text{Pr}_2\text{NiO}_{4+\delta}$ has been revealed to be of unprecedented complexity.²² For the freshly prepared oxide in air, an extra oxygen stoichiometry of $\delta = 0.25$ is obtained, adopting a monoclinic symmetry. Subsequent storing under ambient conditions for several months, yields a topotactic oxygen release towards $\text{Pr}_2\text{NiO}_{4.225}$. Being the ground state for $\text{Pr}_2\text{NiO}_{4+\delta}$ at ambient conditions, this line phase shows a 3D modulated structure, the modulation vector being $\mathbf{Q}_n = \pm 5/6\mathbf{a}^* + 1/2\mathbf{b}^*$. $\text{Pr}_2\text{NiO}_{4.225}$ was consequently used as the starting phase for the electrochemically performed reduction towards the stoichiometric $\text{Pr}_2\text{NiO}_{4.0}$ outlined below. A more detailed crystallographic description of the modulation vectors is discussed in Fig. S3.

The reconstructed (hk0)-plane of the $\text{Pr}_2\text{NiO}_{4.225}$ starting phase is given in Fig. 2a, revealing 4 orthorhombic twin domains with different volume fractions. This can be unambiguously concluded from the specific splitting and intensity ratio of the basic reflections of the parent orthorhombic framework with $Fmmm$ space group (see Fig. 2a-c). All satellite reflections can be indexed with the $\mathbf{Q}_n = \pm 5/6\mathbf{a}^* + 1/2\mathbf{b}^*$ modulation vector as further outlined in ref²². A closer inspection of the integrated, individual intensities of the basic reflections reveals the existence of two main and two minor twin domains with a ratio of the corresponding volume fractions of $\approx 4:44:3:49$ for D1-D4 respectively. The corresponding simulated pattern (Fig. 2b) considers the

positions of basic and satellite reflections with respect to the orthorhombic and monoclinic twinning as outlined in Fig. S2. From the size of the crystal, its mass is determined to be 25.2 μg , which would require a current of 35.2 nA, involving a charge transfer of 0.45 e⁻/f, for a total reaction time of 24h following the reaction equation:



The formally generated O²⁻ ions will instantly decompose together with one water molecule into OH⁻, following O²⁻ + H₂O → 2OH⁻. All attempts to control the reaction (given in (eq.1)) in a galvanostatic reaction mode failed, as a current in the nA region is required. Such low current conditions did not even lead to a partial reduction of Pr₂NiO_{4.225}, most probably due to uncontrollable parasitic reactions which are always present during electrochemical charge/discharge and increasingly dominate over the main electrochemical reaction. The complete reduction towards the stoichiometric Pr₂NiO_{4.0} phase could, however, easily be obtained imposing a current of 10 μA , within a time window of less than 20 h. Such a high reaction kinetics appears to be surprising and interesting as such, but also implies that the auto-balanced reaction kinetics no longer allows to correlate the charge transfer with the oxygen stoichiometry. The required current density thereby amounts to about 15 $\mu\text{A}/\text{cm}^2$, which is remarkably high, considering oxygen ions as the diffusing species together with the single crystalline nature of the electrode material.

Reconstructed (*hk0*)-diffraction planes obtained during the discharge reaction are given in Fig S4, while positional and intensity changes of the (*600/060*) reflection group are illustrated in Fig. 3 a-o. From these reconstructed sections, the contributions of 4 different twin domains are evidenced, which are separated in ω and θ , following the orthorhombic twinning scheme further

outlined in Fig. S2. The crystal twinning and respective reflection splitting presents here a decisive advantage, offering a direct access to a unique and quantitative information of changes in the orthorhombicity as well as the volume fractions of the individual twin domains during the electrochemical reaction. This becomes possible as the structure factor of $(h00)$ and respective $(0h0)$ reflections are almost similar for both orthorhombic phases, as the corresponding scattering differences are related to minor shifts of low- Z oxygen atoms, linked to the tilt of the NiO_6 octahedra around $[100]$.

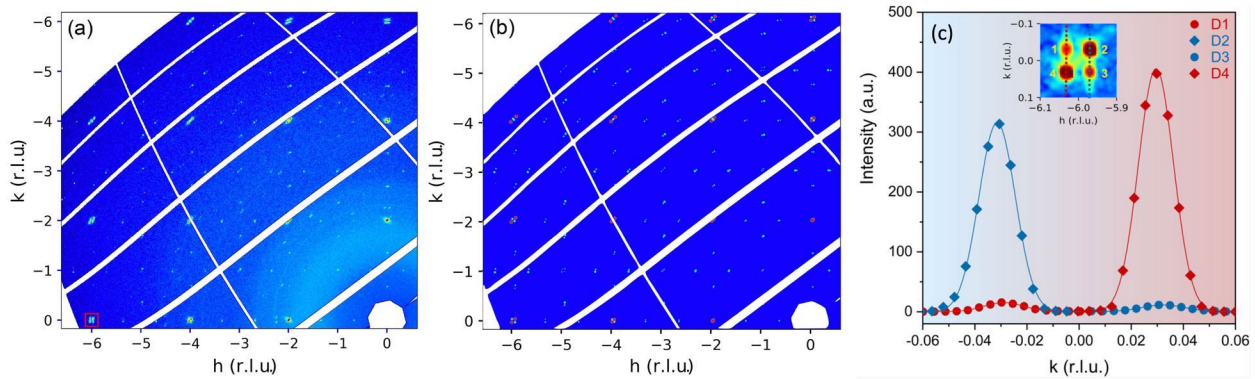


Figure 2a-c. (a) Reconstructed $(hk0)$ -plane of $\text{Pr}_2\text{NiO}_{4.225}$, indicating 4 orthorhombic twin individuals; each orthorhombic twin domain can develop up to four individual monoclinic twin domains. The corresponding simulation of the positions of basic and satellite reflections with respect to their volume fractions is given in (b), taking into account a monoclinic symmetry with a modulation vector $\mathbf{Q}_n = \pm 5/6\mathbf{a}^* + 1/2\mathbf{b}^*$.²² Basic reflections are indicated by a larger spot size. (c): Intensities of the $(600)/(060)$ reflections, obtained from the transversal scans (dotted lines in the inset) for the four twin individuals. The inset is showing the respective reflections, corresponding to the zone marked by a red square in Fig. 2(a). Non-indexed reflections belong without exception to epitaxially grown NiO as outlined in Fig. S5a-b.

As discussed above, the $\text{Pr}_2\text{NiO}_{4.225}$ starting phase shows two main (D2 and D4) and two minor (D1 and D3) domains (Fig. 2c). Since the lattice parameters, and consequently the reflection splitting, vary during the reaction, a comparison of the diffraction planes using individually determined orientation matrices (OM) is not directly applicable. It is, however, possible to make a uniform comparison of all diffraction planes by applying to all reconstructions the same orientation matrix, as given in Fig 3g from the tetragonal intermediate phase. The first six diffraction patterns (*a-f*) show the transition from the orthorhombic starting to the tetragonal intermediate phase. A co-existence of both phases, in agreement with a two-phase reaction step, can be concluded from their integrated intensities as well as from their respective positions. From ref²² it is also evident that already minor variations in the oxygen stoichiometry are supposed to result into significant changes of the modulation vector and thus engendering different satellite reflection positions. The absence of any positional changes confirms $\text{Pr}_2\text{NiO}_{4.225}$ to be a true line phase and the transition towards the tetragonal intermediate phase is strictly following a two-phase reaction mechanism.

Beside the formation of the tetragonal phase, which has been described to adopt the $P4_2/nm$ space group²¹, the appearance of *P*-type reflections during the reduction is observed, while all satellite reflections of the starting phase continuously vanish. Beyond the tetragonal intermediate phase, the reaction further proceeds towards the fully reduced stoichiometric $\text{Pr}_2\text{NiO}_{4.0}$ phase in a two-phase reaction step. The latter shows a strong transversal and longitudinal splitting of the four twin domains, related to the increased orthorhombic deformation. The ortho/tetra/ortho symmetry sequence is, however, accompanied by a considerable change in the volume fractions of all twin individuals comparing the starting and fully reduced $\text{Pr}_2\text{NiO}_{4.0}$ phase as outlined in Fig. 3

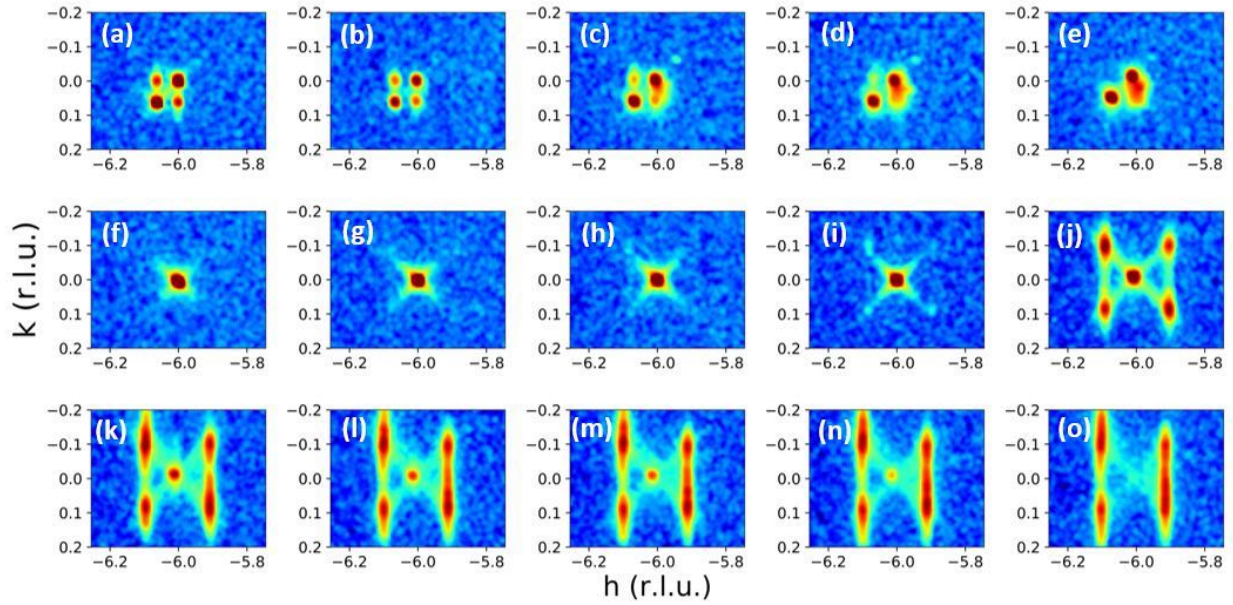


Figure 3 (a-o). Evolution of the positions and intensities of the 4 twin domains, shown for the (600/060) reflections through the orthorhombic/tetragonal/orthorhombic symmetry change, in course of the electrochemical reduction of $\text{Pr}_2\text{NiO}_{4.225}$. All figures have been obtained using the same orienting matrix, i.e., as obtained for the tetragonal intermediate phase (f), allowing to compare absolute positional shifts. A series of the entire (hk0)-diffraction planes is given in Fig S4.

The intensity repartition for all four twin domains shows a clear inversion of the respective intensity ratio between the starting and final phases. The initially weak twin domains D1 and D3 strongly increase in reflection intensity, finally exceeding the initially strong domains D2 and D4. For $\text{Pr}_2\text{NiO}_{4.0}$, the volume fractions for the twin domains D1-D4 yield a final intensity ratio of 32:14:38:16 respectively (Fig. 4). The evolution of all twin domains vs. time is given in the S-media file.

The twin domain structure and formation, related to the ortho/tetra/ortho symmetry sequence also allows to analyze straightforwardly the evolution of the respective volume fractions, and thus, to access to the evolution of the microstructure. From the established volume fractions discussed above, the formation of nano-domains can be ruled out as it would imply an even distribution for the volume fractions of 25% each. Instead, the twin-domain structure encountered here, is very specific. This is also evidenced by the diffuse scattering illustrated in Fig. 3. The (600)-reflection of the tetragonal intermediate phase shows diffuse contributions along the [110]/[-110] directions over the whole non-stoichiometric region, relating the (600) and (060) reflections of all involved twin domains (see Fig. 3j).

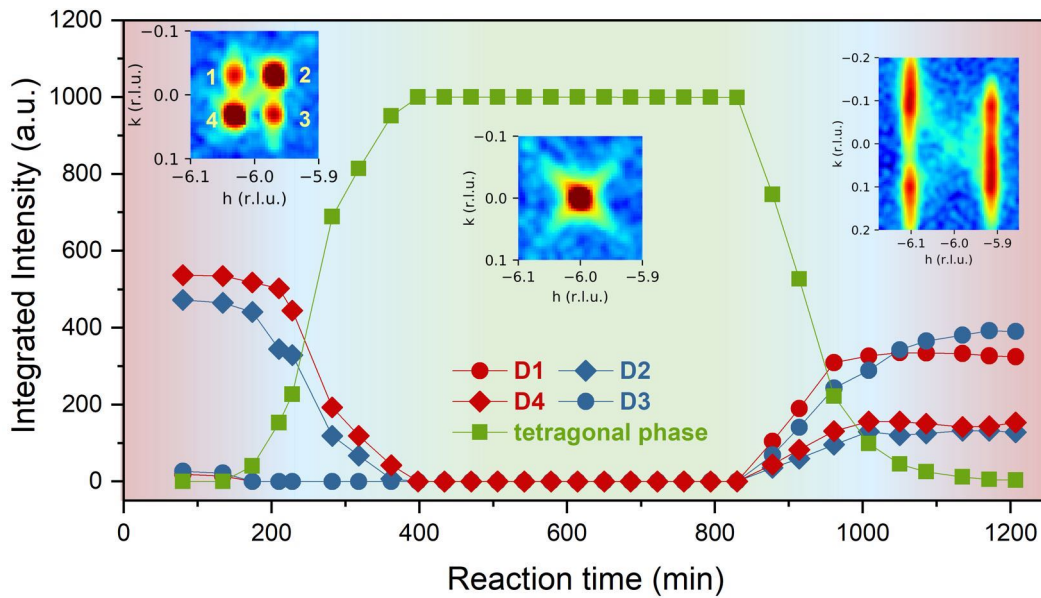


Figure 4. Time dependent evolution of the integrated intensities of the (600/060)-reflections of the 4 twin individuals, indicating a complete inversion of their respective volume fractions before and beyond the tetragonal phase. All errors are within the size of the symbols. A series of the entire (hk0)-diffraction planes is given in Fig S4.

Further on, diffuse scattering becomes visible at the beginning of the transformation from the tetragonal intermediate towards the stoichiometric $\text{Pr}_2\text{NiO}_{4.0}$ phase, relating both, the equivalent (600) reflections of twin domains D2 and D3 as well as (060) reflections of twin domains D1 and D4 respectively. No diffuse scattering is, however, observed between (600) and (060) reflections along the same longitudinal reciprocal lattice direction. Such a behavior is untypical, strongly suggesting that only domains of different twin individuals but same d -values, get averaged on a length scale within the correlation length of X-ray diffraction. It suggests the formation of strongly anisotropic twin domains, which are well defined within the (a,b)-layer but showing a strong stacking disorder of differently oriented domains along the c-axis. Equivalent (h00) as well as (0k0) reflections are nicely defined in the early stage of the formation of the orthorhombic $\text{Pr}_2\text{NiO}_{4.0}$ -phase (Fig3j) for all twin domains, but merge continuously upon further reduction (Fig 3k-o). The twin domain evolution of the (hk4)-plane, equally showing the corresponding reflection conditions of the reduced $\text{Pr}_2\text{NiO}_{4.0}$ phase is given in Fig 5a-f.

These observations are different to what is usually observed for the thermally induced twin domain formation related to the symmetry reduction, following a 2nd order phase transition. The well-established twin-domains along the (a,b)-plane, i.e. parallel to the Pr_2O_2 rock salt layer, indicate that rapid oxygen diffusion may be considered as a process that makes the formation of numerous domain borders along the principal diffusion pathway to be energetically unfavorable.

Further on, additional satellite reflections emerge for several (hkl)-reflections along the [110]-direction (see Fig. 6i-o) at the very first appearance of the stoichiometric $\text{Pr}_2\text{NiO}_{4.0}$. Their positions with respect to the respective basic reflections reveal a periodicity of about 7 nm, remaining invariant upon further reduction. The satellite reflections indicate a coherent domain scattering, similar to what has been reported for ordered nano-domains in ferroelectric superlattices with 180°

domain ordering.²⁸⁻³⁰ In the absence of ferroelectricity for $\text{Pr}_2\text{NiO}_{4.0}$, the most reasonable explanation for domain ordering would be the formation of anti-phase domains involving different octahedra tilting (see Fig S7).

These findings are the first indication for a domain organization, emerging during an electrochemical reaction at RT. Thereby a length scale of translational periodicities corresponding to more than 12 times the unit cell parameters, significantly differs from an averaged domain distribution. From this perspective, the diffusion process, normally considered as a local process, can be seen at larger scale as an anisotropic “field” that optimizes structural features at the macroscopic level of the domain structure. The long-range oxygen-ordering phenomena found for $\text{Pr}_2\text{NiO}_{4+\delta}$,²² deliver, together with the ordering processes of the domains, a clear evidence for the existence of mesoscopic interactions at both, structural and domain level, thus giving a first meaningful descriptor to better understand to what is generally discussed as *domain engineering*.

Due to the fast reaction kinetics, one may assume that the high current applied throughout the reaction, will induce the formation of a phase gradient and/or inhomogeneities from the crystal surface to its inner part for kinetical reasons. A very homogeneously discharge of the entire crystal is instead observed throughout the whole reaction. It implies that the phase formation and stability during oxygen release is strongly aligned with the applied potential, which is supposed to be uniform all over the crystal related to the high metallic conductivity of $\text{Pr}_2\text{NiO}_{4+\delta}$.

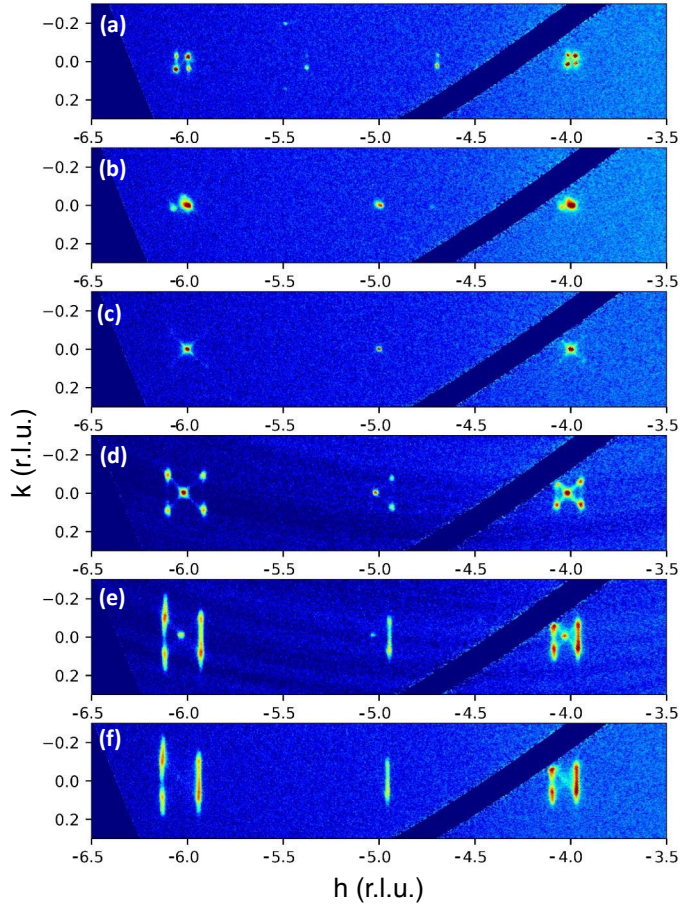


Figure 5. Reflection conditions, formation, and splitting for a characteristic section of the $(hk4)$ -plane. For the starting compound $\text{Pr}_2\text{NiO}_{4.225}$ the basic reflection groups $(404/044)$ and $(604)/(064)$ appear together with satellite reflection related to oxygen ordering in Fig. 5(a), while a newly formed P-type (504) -reflection emerges with the formation of the tetragonal phase in Fig. 5(b-c), in agreement with the $P4_2/nm$ space group. With the formation of the stoichiometric $\text{Pr}_2\text{NiO}_{4.0}$ phase (Fig. 5d-f), all basic reflections split up to four newly formed $(h04)/(0h4)$ orthorhombic twin domains, while the (504) reflection, which is a unique reflection for the tetragonal phase, transforms into two (054) reflections related to twin domains D2 and D3, the corresponding (504) reflections being absent by symmetry. The (054) reflections are allowed in the space group $Bmab$, while forbidden in $Abma$, for the corresponding orthorhombic twin domains inverted around $[110]/[-110]$ (see Fig S2).

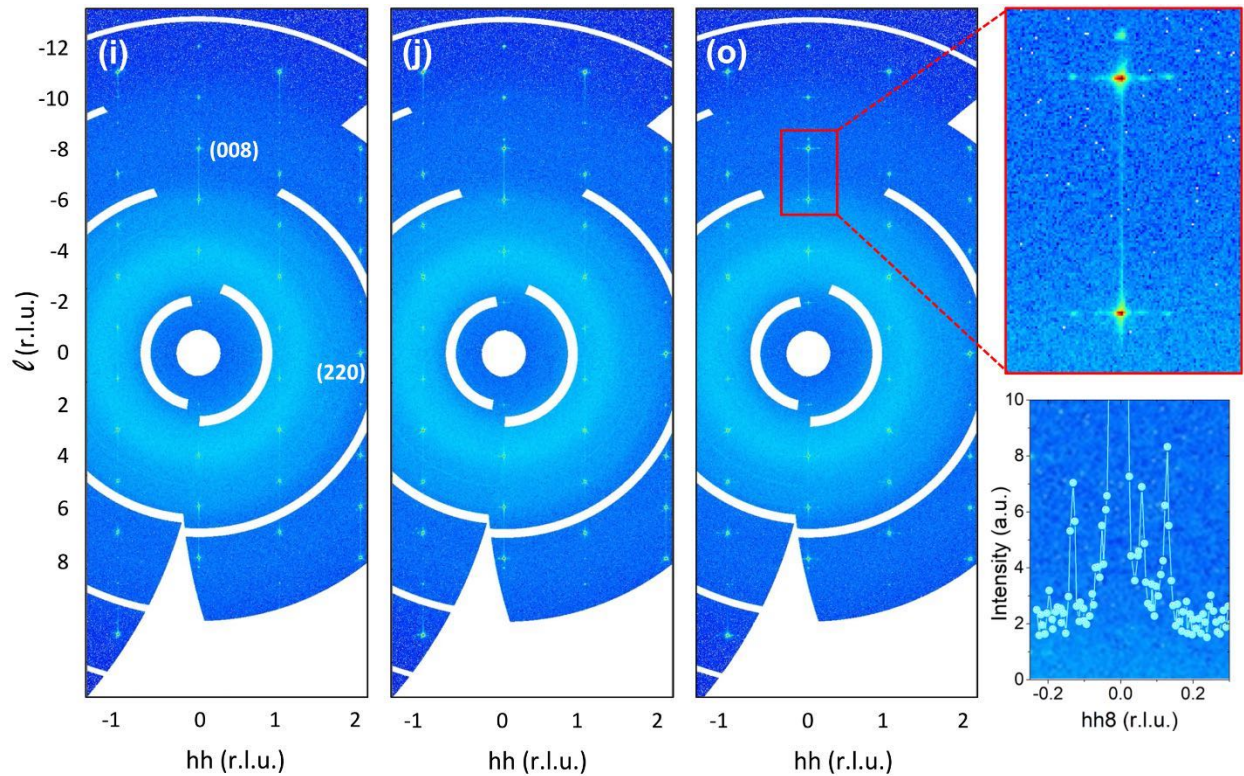


Figure 6. Reconstructed (hhl)-planes for $\text{Pr}_2\text{NiO}_{4+\delta}$ phases during the electrochemical reduction, the numbering corresponds to the figures listed in Figs 3 and S4. Satellite reflections indicating a periodicity of about 7 nm along [110] become evident for the fully reduced phase (o), while essentially absent for the pure tetragonal phase (i). For clarity, the satellites belonging to the (006) and (008) reflections are outlined with a red frame in the zoomed section of Fig. 6(o). The extra reflections do not belong to the stoichiometric orthorhombic $\text{Pr}_2\text{NiO}_{4.0}$ phase, but are indicative for coherent twin domain scattering, related to the complex twin domain structure involving stratified layer disorder. The intensities of the satellite reflections around the (008) reflections are given along the (hh8)-direction, indicating the formation of up to 2nd order harmonics.

Given that the entire electrochemical reduction proceeds in less than 20 hours, the related diffusion coefficient along the [110] direction can be accessed from the crystal dimensions and orientation. With the c-axis corresponding to the long rotation axis, the oxygen diffusion length along the [110] diffusion pathway consequently amounts to half of the crystal diameter, i.e. 30 μm . Following the simplified equation, considering a one-dimensional random walk diffusion of particles $\langle x^2 \rangle = 2Dt$,³¹ the overall effective diffusion coefficient would then correspond to $D^* = 6.3 \times 10^{-11} \text{ cm}^2\text{s}^{-1}$. This value appears to be remarkably high although not directly comparable to the standard chemical diffusion coefficient, as it is obtained under applied electrochemical potential. Nevertheless, it roughly reflects the corresponding effective oxygen transport which is, however, similar to oxygen diffusion coefficients in solid oxides usually encountered above 600-800°C. Only a very few cases have been reported with unusually high oxygen diffusion coefficients at ambient, i.e. polycrystalline $\text{Nd}_{1-x}\text{Sr}_x\text{CoO}_3$, $\text{La}_2\text{CoO}_{4+\delta}$ and $\text{La}_2\text{CuO}_{4+\delta}$.³²⁻³⁴ Oxygen diffusion coefficients as high as $2 \times 10^{-8} \text{ cm}^2\text{s}^{-1}$ were reported by the $^{18}\text{O}/^{16}\text{O}$ tracer diffusion method for $\text{La}_2\text{Ni}_{1-x}\text{Co}_x\text{O}_{4+d}$ and $\text{Pr}_2\text{NiO}_{4+\delta}$ at 500°C.^{27, 35}

For $\text{Pr}_2\text{NiO}_{4+\delta}$ the T-dependence of D^* obtained by the isotope tracer diffusion method²⁷ can be extrapolated to $D^* \approx 10^{-15} \text{ cm}^2\text{s}^{-1}$ at ambient temperature (see Fig S6). The effective oxygen mass transport obtained here under applied electrochemical potential at RT, importantly reveals a diffusion coefficient of more than 4 orders of magnitude higher, clearly evidencing the potential of single crystalline electrodes for oxygen diffusion at ambient conditions.

Only a few examples of oxygen diffusion investigated using single crystals or epitaxial thin films by *in situ* diffraction methods. Thermally induced oxygen uptake/release reactions have also been studied on epitaxially grown non-stoichiometric SrCoO_{3-x} thin films with a thickness of 30-60 nm.³⁶ The revealed oxygen diffusion at 300°C, as indicated by the reversible switching of

Brownmillerite-type $\text{SrCoO}_{2.5}$ towards the cubic SrCoO_{3-x} perovskite framework, has been reported to proceed quantitatively in about one minute. Given the diffusion pathway of 30 nm, these diffusion values correspond exactly to what is obtained for the electrochemical reduction of single crystalline $\text{Pr}_2\text{NiO}_{4+\delta}$ electrodes with $30\mu\text{m}$ crystal radius and a reduction time of 20 h. The difference is that the electrochemical reaction on $\text{Pr}_2\text{NiO}_{4+\delta}$ is performing at ambient conditions, while the thickness of the used crystal is clearly indicating the oxygen diffusion to be a true bulk property.

We also note that the reaction time obtained on $\text{Pr}_2\text{NiO}_{4+\delta}$ single crystalline electrodes is about 5 times faster compared to polycrystalline electrodes when running under equilibrium conditions.²¹ The same also holds for the electrochemical oxidation of polycrystalline electrodes of $\text{SrFeO}_{2.5}$ and $\text{SrCoO}_{2.5}$.^{37,38}

CONCLUSIONS

Using single crystalline $\text{Pr}_2\text{NiO}_{4.225}$ electrodes, we observed an impressively fast reaction kinetics during the reduction towards stoichiometric $\text{Pr}_2\text{NiO}_{4.0}$. Our results suggest that the reduced amount of grain boundaries in single crystalline material presents a tremendous advantage to reach high diffusion rates. A complex microstructure was evidenced with the appearance of satellite reflections, indicating long-range periodicities of 7 nm along [110], related to anti phase domains along the oxygen diffusion pathway. We thus observed a hierarchy of large-scale oxygen and domain periodicities, associated with twinning or structural modulations linked to stoichiometry, on the scale of tens of nano-meters and larger. This observation, together with a control of the large-scale periodicity via stoichiometry, shows that these materials, in a certain range of compositions, may be seen as periodic multi-layer dielectric stacks – photonic crystals, and

therefore be of interest for application in the field of photonic devices that can modulate and process light signals³⁹. In this context it is interesting to note that pure stoichiometric Pr₂NiO_{4.0} crystals, as we could obtain recently for the first time, are fully transparent.

Our results clearly underline that oxygen diffusion mechanisms performing at ambient temperature are obviously more complex and far from being seen as a single particle hopping process. Phenomenologically, these results present a promising approach for stand-alone single crystalline electrodes to be used for oxygen membranes/electrolytes or oxygen sensor material, also related to their stronger mechanical performance compared to sintered electrodes.

Finally, we want to underline the importance of high resolution *in-situ* single crystal diffraction carried out at performant single crystal diffractometers using low noise 2D area detectors, which is decisive to obtain high-resolution maps of the reciprocal space, thus accessing information, that goes beyond to what classical powder diffraction methods can provide.

Supporting Information. The following files are available free of charge:

Additional experimental details, structural characterizations, and oxygen diffusion data, including a scheme and a photo of the experimental setup.

In the mov file, a time resolved evolution of characteristic single crystal reflection profiles throughout the electrochemical reduction are provided.

AUTHOR INFORMATION

Corresponding Author

[*werner.paulus@umontpellier.fr](mailto:werner.paulus@umontpellier.fr)

Present Addresses

‡ Heinz Maier-Leibnitz Zentrum (MLZ), Technische Universität München, 85747 Garching, Germany

‡ Institut für Kristallographie, RWTH Aachen, Jägerstrasse 17-19, 52056 Aachen, Germany, Outstation at Heinz Maier-Leibnitz Zentrum, FRMII, Lichtenbergstrasse 1, 85747 Garching, Germany

& NRC-Nanotechnology Research Centre, Edmonton, AB, Canada T6G 2M9

Funding Sources

Financial support from the French National Research Agency (ANR) through the project “Structural induced Electronic Complexity controlled by low temperature Topotactic Reaction” (SECTOR No. ANR-14-CE36-0006-01) is gratefully acknowledged. The PhD contract of A.M. was provided by the French ministry of Research and Education (MENRT)

ACKNOWLEDGMENT

The authors acknowledge the beam times used at beamline BM01@SNBL at the European Synchrotron Radiation Facility (ESRF, Grenoble) and the “Plateforme d’Analyse et de Caractérisation” of the ICG Montpellier.

REFERENCES

(1) Shao, Z.; Haile, S. M. A high-performance cathode for the next generation of solid-oxide fuel cells. *Nature* **2004**, *431* (7005), 170-173. DOI: 10.1038/nature02863.

(2) Huang, Y.-H.; Dass, R. I.; Xing, Z.-L.; Goodenough, J. B. Double Perovskites as Anode Materials for Solid-Oxide Fuel Cells. *Science* **2006**, *312* (5771), 254. DOI: 10.1126/science.1125877.

(3) Sunarso, J.; Baumann, S.; Serra, J. M.; Meulenberg, W. A.; Liu, S.; Lin, Y. S.; Diniz da Costa, J. C. Mixed ionic–electronic conducting (MIEC) ceramic-based membranes for oxygen separation. *Journal of Membrane Science* **2008**, *320* (1), 13-41. DOI: <https://doi.org/10.1016/j.memsci.2008.03.074>.

(4) Lacorre, P.; Goutenoire, F.; Bohnke, O.; Retoux, R.; Laligant, Y. Designing fast oxide-ion conductors based on $\text{La}_2\text{Mo}_2\text{O}_9$. *Nature* **2000**, *404* (6780), 856-858. DOI: 10.1038/35009069.

(5) Garbayo, I.; Chiabrera, F.; Alayo, N.; Santiso, J.; Morata, A.; Tarancón, A. Thin film oxide-ion conducting electrolyte for near room temperature applications. *Journal of Materials Chemistry A* **2019**, *7* (45), 25772-25778, 10.1039/C9TA07632H. DOI: 10.1039/C9TA07632H.

(6) Chronos, A.; Yildiz, B.; Tarancón, A.; Parfitt, D.; Kilner, J. A. Oxygen diffusion in solid oxide fuel cell cathode and electrolyte materials: mechanistic insights from atomistic simulations. *Energy & Environmental Science* **2011**, *4* (8), 2774-2789, 10.1039/C0EE00717J. DOI: 10.1039/C0EE00717J.

(7) Chiabrera, F.; Garbayo, I.; López-Conesa, L.; Martín, G.; Ruiz-Caridad, A.; Walls, M.; Ruiz-González, L.; Kordatos, A.; Núñez, M.; Morata, A.; et al. Engineering Transport in Manganites by Tuning Local Nonstoichiometry in Grain Boundaries. *Advanced Materials* **2019**, *31* (4), 1805360,

<https://doi.org/10.1002/adma.201805360>. DOI: <https://doi.org/10.1002/adma.201805360>

(accessed 2021/04/23).

(8) Saranya, A. M.; Morata, A.; Pla, D.; Burriel, M.; Chiabrera, F.; Garbayo, I.; Hornés, A.; Kilner, J. A.; Tarancón, A. Unveiling the Outstanding Oxygen Mass Transport Properties of Mn-Rich Perovskites in Grain Boundary-Dominated $\text{La}_{0.8}\text{Sr}_{0.2}(\text{Mn}_{1-x}\text{Co}_x)_{0.85}\text{O}_{3+\delta}$ Nanostructures. *Chemistry of Materials* **2018**, *30* (16), 5621-5629. DOI: 10.1021/acs.chemmater.8b01771.

(9) Navickas, E.; Huber, T. M.; Chen, Y.; Hetaba, W.; Holzlechner, G.; Rupp, G.; Stöger-Pollach, M.; Friedbacher, G.; Hutter, H.; Yildiz, B.; et al. Fast oxygen exchange and diffusion kinetics of grain boundaries in Sr-doped LaMnO_3 thin films. *Physical Chemistry Chemical Physics* **2015**, *17* (12), 7659-7669, 10.1039/C4CP05421K. DOI: 10.1039/C4CP05421K.

(10) Ceretti, M.; Wahyudi, O.; Cousson, A.; Villesuzanne, A.; Meven, M.; Pedersen, B.; Bassat, J. M.; Paulus, W. Low temperature oxygen diffusion mechanisms in $\text{Nd}_2\text{NiO}_{4+\delta}$ and $\text{Pr}_2\text{NiO}_{4+\delta}$ via large anharmonic displacements, explored by single crystal neutron diffraction. *Journal of Materials Chemistry A* **2015**, *3* (42), 21140-21148, 10.1039/C5TA05767A. DOI: 10.1039/C5TA05767A.

(11) Paulus, W.; Schober, H.; Eibl, S.; Johnson, M.; Berthier, T.; Hernandez, O.; Ceretti, M.; Plazanet, M.; Conder, K.; Lamberti, C. Lattice Dynamics To Trigger Low Temperature Oxygen Mobility in Solid Oxide Ion Conductors. *Journal of the American Chemical Society* **2008**, *130* (47), 16080-16085. DOI: 10.1021/ja806144a.

(12) Perrichon, A.; Piovano, A.; Boehm, M.; Zbiri, M.; Johnson, M.; Schober, H.; Ceretti, M.; Paulus, W. Lattice Dynamics Modified by Excess Oxygen in $\text{Nd}_2\text{NiO}_{4+\delta}$: Triggering Low-

Temperature Oxygen Diffusion. *The Journal of Physical Chemistry C* **2015**, *119* (3), 1557-1564. DOI: 10.1021/jp510392h.

(13) Piovano, A.; Perrichon, A.; Boehm, M.; Johnson, M. R.; Paulus, W. Positional recurrence maps, a powerful tool to de-correlate static and dynamical disorder in distribution maps from molecular dynamics simulations: the case of $\text{Nd}_2\text{NiO}_{4+\delta}$. *Physical Chemistry Chemical Physics* **2016**, *18* (26), 17398-17403, 10.1039/C5CP06464C. DOI: 10.1039/C5CP06464C.

(14) Villesuzanne, A.; Paulus, W.; Cousson, A.; Hosoya, S.; Le Dréau, L.; Hernandez, O.; Prestipino, C.; Ikbél Houchati, M.; Schefer, J. On the role of lattice dynamics on low-temperature oxygen mobility in solid oxides: a neutron diffraction and first-principles investigation of $\text{La}_2\text{CuO}_{4+\delta}$. *Journal of Solid State Electrochemistry* **2011**, *15* (2), 357-366. DOI: 10.1007/s10008-010-1274-7.

(15) Li, X.; Benedek, N. A. Enhancement of Ionic Transport in Complex Oxides through Soft Lattice Modes and Epitaxial Strain. *Chemistry of Materials* **2015**, *27* (7), 2647-2652. DOI: 10.1021/acs.chemmater.5b00445.

(16) Magro, F.; Ceretti, M.; Meven, M.; Paulus, W. Infrared furnace for in situ neutron single-crystal diffraction studies in controlled gas atmospheres at high temperatures. *Journal of Applied Crystallography* **2021**, *54* (3), 822-829. DOI: doi:10.1107/S1600576721003198.

(17) Kushima, A.; Parfitt, D.; Chroneos, A.; Yildiz, B.; Kilner, J. A.; Grimes, R. W. Interstitialcy diffusion of oxygen in tetragonal $\text{La}_2\text{CoO}_{4+\delta}$. *Physical Chemistry Chemical Physics* **2011**, *13* (6), 2242-2249, 10.1039/C0CP01603A. DOI: 10.1039/C0CP01603A.

(18) Parfitt, D.; Chronos, A.; Kilner, J. A.; Grimes, R. W. Molecular dynamics study of oxygen diffusion in $\text{Pr}_2\text{NiO}_{4+\delta}$. *Physical Chemistry Chemical Physics* **2010**, *12* (25), 6834-6836, 10.1039/C001809K. DOI: 10.1039/C001809K.

(19) Yashima, M.; Yamada, H.; Nuansaeng, S.; Ishihara, T. Role of Ga^{3+} and Cu^{2+} in the High Interstitial Oxide-Ion Diffusivity of Pr_2NiO_4 -Based Oxides: Design Concept of Interstitial Ion Conductors through the Higher-Valence d^{10} Dopant and Jahn–Teller Effect. *Chemistry of Materials* **2012**, *24* (21), 4100-4113. DOI: 10.1021/cm3021287.

(20) Yashima, M.; Enoki, M.; Wakita, T.; Ali, R.; Matsushita, Y.; Izumi, F.; Ishihara, T. Structural Disorder and Diffusional Pathway of Oxide Ions in a Doped Pr_2NiO_4 -Based Mixed Conductor. *Journal of the American Chemical Society* **2008**, *130* (9), 2762-2763. DOI: 10.1021/ja711478h.

(21) Ceretti, M.; Wahyudi, O.; André, G.; Meven, M.; Villesuzanne, A.; Paulus, W. $(\text{Nd/Pr})_2\text{NiO}_{4+\delta}$: Reaction Intermediates and Redox Behavior Explored by in Situ Neutron Powder Diffraction during Electrochemical Oxygen Intercalation. *Inorganic Chemistry* **2018**, *57* (8), 4657-4666. DOI: 10.1021/acs.inorgchem.8b00393.

(22) Dutta, R.; Maity, A.; Marsicano, A.; Ceretti, M.; Chernyshov, D.; Bosak, A.; Villesuzanne, A.; Roth, G.; Perversi, G.; Paulus, W. Long-range oxygen ordering linked to topotactic oxygen release in $\text{Pr}_2\text{NiO}_{4+\delta}$ fuel cell cathode material. *Journal of Materials Chemistry A* **2020**, *8* (28), 13987-13995, 10.1039/D0TA04652C. DOI: 10.1039/D0TA04652C.

(23) Ceretti, M.; Piovano, A.; Cousson, A.; Berthier, T.; Meven, M.; Agostini, G.; Schefer, J.; Hernandez, O.; Lamberti, C.; Paulus, W. Growth and characterization of large high quality

brownmillerite $\text{CaFeO}_{2.5}$ single crystals. *CrystEngComm* **2012**, *14* (18), 5771-5776, 10.1039/C2CE25413A. DOI: 10.1039/C2CE25413A.

(24) Wahyudi, O.; Ceretti, M.; Weill, I.; Cousson, A.; Weill, F.; Meven, M.; Guerre, M.; Villesuzanne, A.; Bassat, J. M.; Paulus, W. Growth of high quality single crystals of strontium doped (Nd,Pr)-nickelates, $\text{Nd}_{2-x}\text{Sr}_x\text{NiO}_{4+\delta}$ and $\text{Pr}_{2-x}\text{Sr}_x\text{NiO}_{4+\delta}$ *Crystengcomm* **2015**, *17* (33), 6278-6285, 10.1039/C5CE00906E. DOI: 10.1039/c5ce00906e.

(25) Maity, A.; Dutta, R.; Penkala, B.; Ceretti, M.; Letrouit-Lebranchu, A.; Chernyshov, D.; Perichon, A.; Piovano, A.; Bossak, A.; Meven, M.; et al. Solid-state reactivity explored in situ by synchrotron radiation on single crystals: from $\text{SrFeO}_{2.5}$ to SrFeO_3 via electrochemical oxygen intercalation. *Journal of Physics D: Applied Physics* **2015**, *48* (50), 504004. DOI: 10.1088/0022-3727/48/50/504004.

(26) Dyadkin, V.; Pattison, P.; Dmitriev, V.; Chernyshov, D. A new multipurpose diffractometer PILATUS@SNBL. *Journal of Synchrotron Radiation* **2016**, *23* (3), 825-829. DOI: doi:10.1107/S1600577516002411.

(27) Bassat, J.-M.; Burriel, M.; Wahyudi, O.; Castaing, R.; Ceretti, M.; Veber, P.; Weill, I.; Villesuzanne, A.; Grenier, J.-C.; Paulus, W.; et al. Anisotropic Oxygen Diffusion Properties in $\text{Pr}_2\text{NiO}_{4+\delta}$ and $\text{Nd}_2\text{NiO}_{4+\delta}$ Single Crystals. *The Journal of Physical Chemistry C* **2013**, *117* (50), 26466-26472. DOI: 10.1021/jp409057k.

(28) Zubko, P.; Stucki, N.; Lichtensteiger, C.; Triscone, J. M. X-Ray Diffraction Studies of 180° Ferroelectric Domains in $\text{PbTiO}_3/\text{SrTiO}_3$ Superlattices under an Applied Electric Field. *Physical Review Letters* **2010**, *104* (18), 187601. DOI: 10.1103/PhysRevLett.104.187601.

(29) Zubko, P.; Jecklin, N.; Torres-Pardo, A.; Aguado-Puente, P.; Gloter, A.; Lichtensteiger, C.; Junquera, J.; Stéphan, O.; Triscone, J. M. Electrostatic Coupling and Local Structural Distortions at Interfaces in Ferroelectric/Paraelectric Superlattices. *Nano Letters* **2012**, *12* (6), 2846-2851. DOI: 10.1021/nl3003717.

(30) Sarott, M. F.; Gradauskaite, E.; Nordlander, J.; Strkalj, N.; Trassin, M. In situ monitoring of epitaxial ferroelectric thin-film growth. *Journal of Physics: Condensed Matter* **2021**, *33* (29), 293001. DOI: 10.1088/1361-648x/abf979.

(31) Einstein, A. Über die von der molekularkinetischen Theorie der Wärme geforderte Bewegung von in ruhenden Flüssigkeiten suspendierten Teilchen. *Annalen der Physik* **1905**, *322* (8), 549-560, <https://doi.org/10.1002/andp.19053220806>. DOI: <https://doi.org/10.1002/andp.19053220806> (accessed 2021/05/14).

(32) Girgsdies, F.; Schöllhorn, R. Spontaneous topotactic oxidation of La_2CoO_4 at room temperature. *Solid State Communications* **1994**, *91* (2), 111-112. DOI: [https://doi.org/10.1016/0038-1098\(94\)90264-X](https://doi.org/10.1016/0038-1098(94)90264-X).

(33) Kudo, T.; Obayashi, H.; Gejo, T. Electrochemical Behavior of the Perovskite-Type $\text{Nd}_{1-x}\text{Sr}_x\text{CoO}_3$ in an Aqueous Alkaline Solution. *Journal of The Electrochemical Society* **1975**, *122* (2), 159-163. DOI: 10.1149/1.2134173.

(34) Grenier, J. C.; Arrouy, F.; Locquet, J. P.; Monroux, C.; Pouchard, M.; Villesuzanne, A.; Wattiaux, A. The Role of The Additional Oxygen Atoms on the Superconducting Properties of La_2CuO_4 -Related Compounds. In *Phase Separation in Cuprate Superconductors: The Role of The Additional Oxygen Atoms on the Superconducting Properties of La_2CuO_4 -Related Compounds*,

Berlin, Heidelberg, 1994//, 1994; Sigmund, E., Müller, K. A., Eds.; Springer Berlin Heidelberg: pp 236-256.

(35) Munnings, C. N.; Skinner, S. J.; Amow, G.; Whitfield, P. S.; Davidson, I. J. Oxygen transport in the $\text{La}_2\text{Ni}_{1-x}\text{Co}_x\text{O}_{4+\delta}$ system. *Solid State Ionics* **2005**, *176* (23), 1895-1901. DOI: <https://doi.org/10.1016/j.ssi.2005.06.002>.

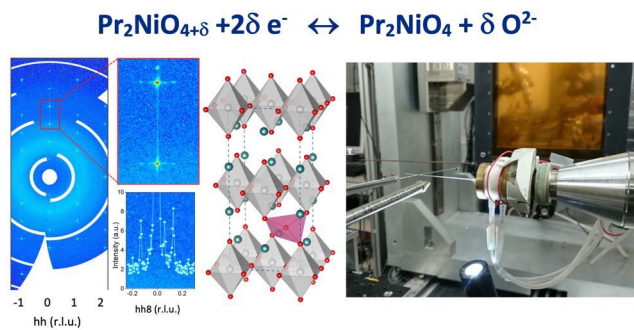
(36) Jeen, H.; Choi, W. S.; Biegalski, M. D.; Folkman, C. M.; Tung, I. C.; Fong, D. D.; Freeland, J. W.; Shin, D.; Ohta, H.; Chisholm, M. F.; et al. Reversible redox reactions in an epitaxially stabilized SrCoO_x oxygen sponge. *Nature Materials* **2013**, *12* (11), 1057-1063. DOI: 10.1038/nmat3736.

(37) Le Toquin, R.; Paulus, W.; Cousson, A.; Prestipino, C.; Lamberti, C. Time-Resolved in Situ Studies of Oxygen Intercalation into $\text{SrCoO}_{2.5}$, Performed by Neutron Diffraction and X-ray Absorption Spectroscopy. *Journal of the American Chemical Society* **2006**, *128* (40), 13161-13174. DOI: 10.1021/ja063207m.

(38) Piovano, A.; Agostini, G.; Frenkel, A. I.; Bertier, T.; Prestipino, C.; Ceretti, M.; Paulus, W.; Lamberti, C. Time Resolved in Situ XAFS Study of the Electrochemical Oxygen Intercalation in $\text{SrFeO}_{2.5}$ Brownmillerite Structure: Comparison with the Homologous $\text{SrCoO}_{2.5}$ System. *The Journal of Physical Chemistry C* **2011**, *115* (4), 1311-1322. DOI: 10.1021/jp107173b.

(39) Joannopoulos John D., J. S. G., Winn Joshua N., Meade Robert D. *Photonic Crystals: Molding the Flow of Light*; Princeton University Press, Princeton, NJ USA, 2008.

Table of Contents. Long-range domain ordering observed by *in situ* single crystal synchrotron diffraction during the electrochemical reduction of $\text{Pr}_2\text{NiO}_{4.225}$ towards $\text{Pr}_2\text{NiO}_{4.0}$ at room temperature showing periodicities of 70 Å.



Supplementary information:

Exploring fast room temperature oxygen diffusion in $\text{Pr}_2\text{NiO}_{4+\delta}$ stand-alone single crystalline electrodes

Avishek Maity^{a,‡}, Rajesh Dutta^{a,‡}, Oles Sendtskyi^{a,‡} & Monica Ceretti^a, Angélique Lebranchu^a, Dmitry Chernyshov^b, Alexei Bosak^c, Werner Paulus^{a*}

Corresponding Author: [*werner.paulus@umontpellier.fr](mailto:werner.paulus@umontpellier.fr)

^a*ICGM, Université Montpellier, CNRS, ENSCM, Montpellier 34095, France*

^b*Swiss-Norwegian Beam Lines at European Synchrotron Radiation Facility, 71 avenue des Martyrs, 38000 Grenoble, France*

^c*European Synchrotron Radiation Facility, 71 avenue des Martyrs, 38000 Grenoble, France*

[‡] *present address: Heinz Maier-Leibnitz Zentrum (MLZ), Technische Universität München, 85747 Garching, Germany*

^{||} *present address: Institut für Kristallographie, RWTH Aachen, Jägerstrasse 17-19, 52056 Aachen, Germany, Outstation at Heinz Maier-Leibnitz Zentrum, FRMII, Lichtenbergstrasse 1, D - 85747 Garching, Germany*

[&] *present address: NRC-Nanotechnology Research Centre, Edmonton, AB, Canada T6G 2M9*

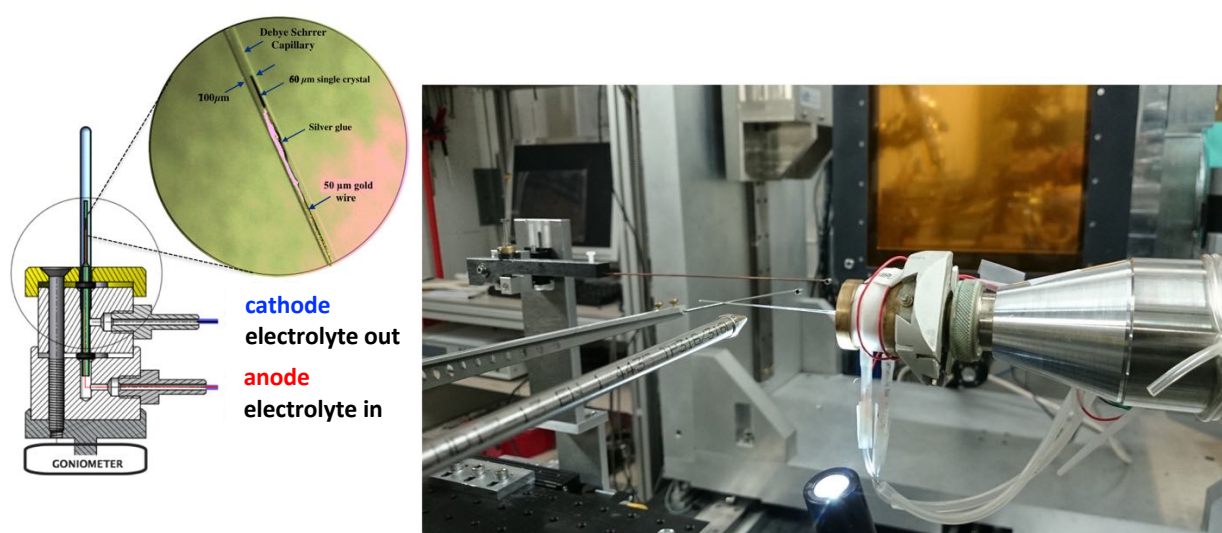


Figure S1: Assembly drawing (left) and experimental setup (right) of the electrochemical cell used for *in situ* single crystal diffraction studies during the electrochemical oxidation of a $\text{Pr}_2\text{NiO}_{4.225}$ single crystal on BM01. The whole cell allows free rotation of 360° , enabling to scan an important part of the whole reciprocal space, suitable for the reconstruction of specific lattice planes. The used crystal of $60 \times 60 \times 1000 \mu\text{m}^3$ was shaped with the c-axis corresponding to the rotation axis, in order to optimize any oxygen diffusion along [110]. Fresh electrolyte is continuously pumped through the inner capillary, and which is open on the top part, enabling to leave over the outer capillary as outlined. The crystal is glued inside the inner capillary on a gold wire with a silver glue. The gold wire is taken out over the electrolyte entrance and serving as anode. The cathode is a $100 \mu\text{m}$ platinum wire which is brought inside the cell over the electrolyte exit.

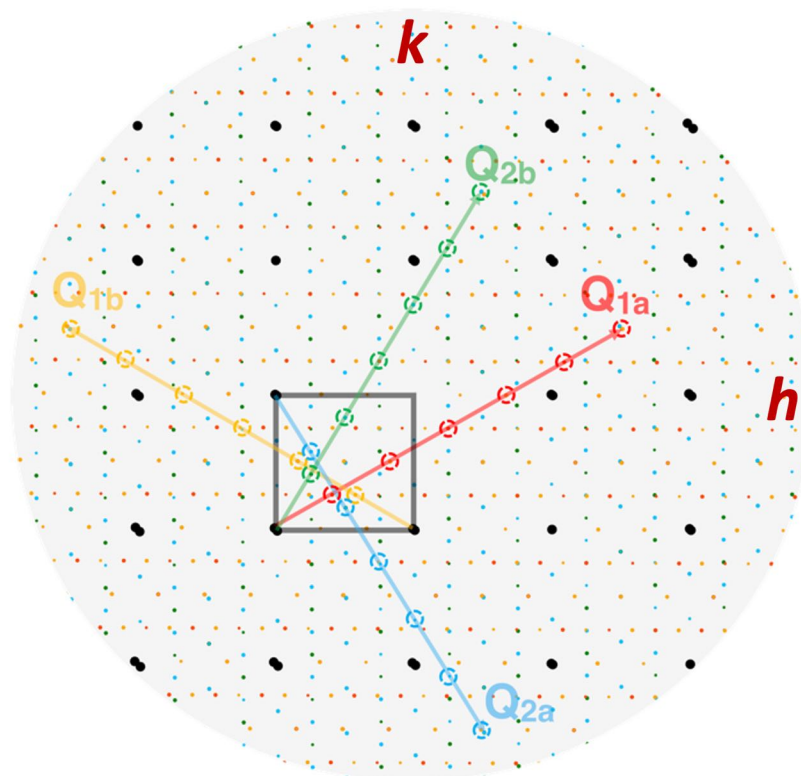


Fig. S3: Simulated diffraction pattern of Pr₂NiO_{4.225} for the commensurate modulation vector $\mathbf{Q}_n = \pm 5/6\mathbf{a}^* + 1/2\mathbf{b}^*$, taking into account 2 orthorhombic twin domains, each forming up to 4 monoclinic domains, which are almost perfectly superimposed due to the minor deviation of the monoclinic angle from 90°. As a consequence all domains result in an almost perfect merohedical overlay of all satellite reflections as further outlined in ref²². The satellite reflections were all assumed to have the same intensity.

As prepared Pr₂NiO_{4+ δ} in air shows an extra oxygen stoichiometry of $\delta = 0.25$ adapting a monoclinic symmetry (space group F112/m, with lattice parameters $a = 5.3977(3) \text{ \AA}$, $b = 5.4540(3) \text{ \AA}$, $c = 12.4362(10) \text{ \AA}$, $\gamma = 90.03^\circ(1)$). Storing under ambient conditions leads to a topotactic release of the O-stoichiometry towards Pr₂NiO_{4.225} with $a = 5.3945(4) \text{ \AA}$, $b = 5.4538(4) \text{ \AA}$, $c = 12.4408(10) \text{ \AA}$, $\gamma = 90.07(1)^\circ$. While the changes in the lattice parameters are only marginal, the respective change of the modulation vector ordering from $\mathbf{Q}_n = \pm 7/9\mathbf{a}^* + 5/9\mathbf{b}^*$ towards $\mathbf{Q}_n = \pm 5/6\mathbf{a}^* + 1/2\mathbf{b}^*$ clearly indicates a distinct oxygen ordering. For Pr₂NiO_{4.25}, the space group of the modulated structure is $P112/m(\alpha\beta 0)(00)$, a subgroup of the standard setting $P2/m$. The oxygen release towards Pr₂NiO_{4.225} yields a different oxygen ordering scheme, resulting in a more complex symmetry with a (3+2)-dimensional super space description. With the general scattering vector $\mathbf{G} = h\mathbf{a}^* + k\mathbf{b}^* + l\mathbf{c}^* + m_1\mathbf{Q}_n + m_2\mathbf{q}_n$ with $0 \leq |m_1| \leq 6$ and $0 \leq |m_2| \leq 1$, n symbolizes the number of the twin individuals, ranging between $1 \leq n \leq 4$. With $\mathbf{q}_n = \pm 0.25\mathbf{a}^* + 0.25\mathbf{b}^* + 0.5\mathbf{c}^*$, the (3+2) super space group thus becomes $P112/m(\alpha_1\beta_1 0)(0s)(\alpha_2\beta_2 1/2)(00)$. Interestingly, both phases appear to be line phases, despite the only narrow difference in their respective oxygen stoichiometry.¹

1. Dutta, R. *et al.* Long-range oxygen ordering linked to topotactic oxygen release in Pr₂NiO_{4+ δ} fuel cell cathode material. *Journal of Materials Chemistry A* **8**, 13987-13995, doi:10.1039/D0TA04652C (2020)

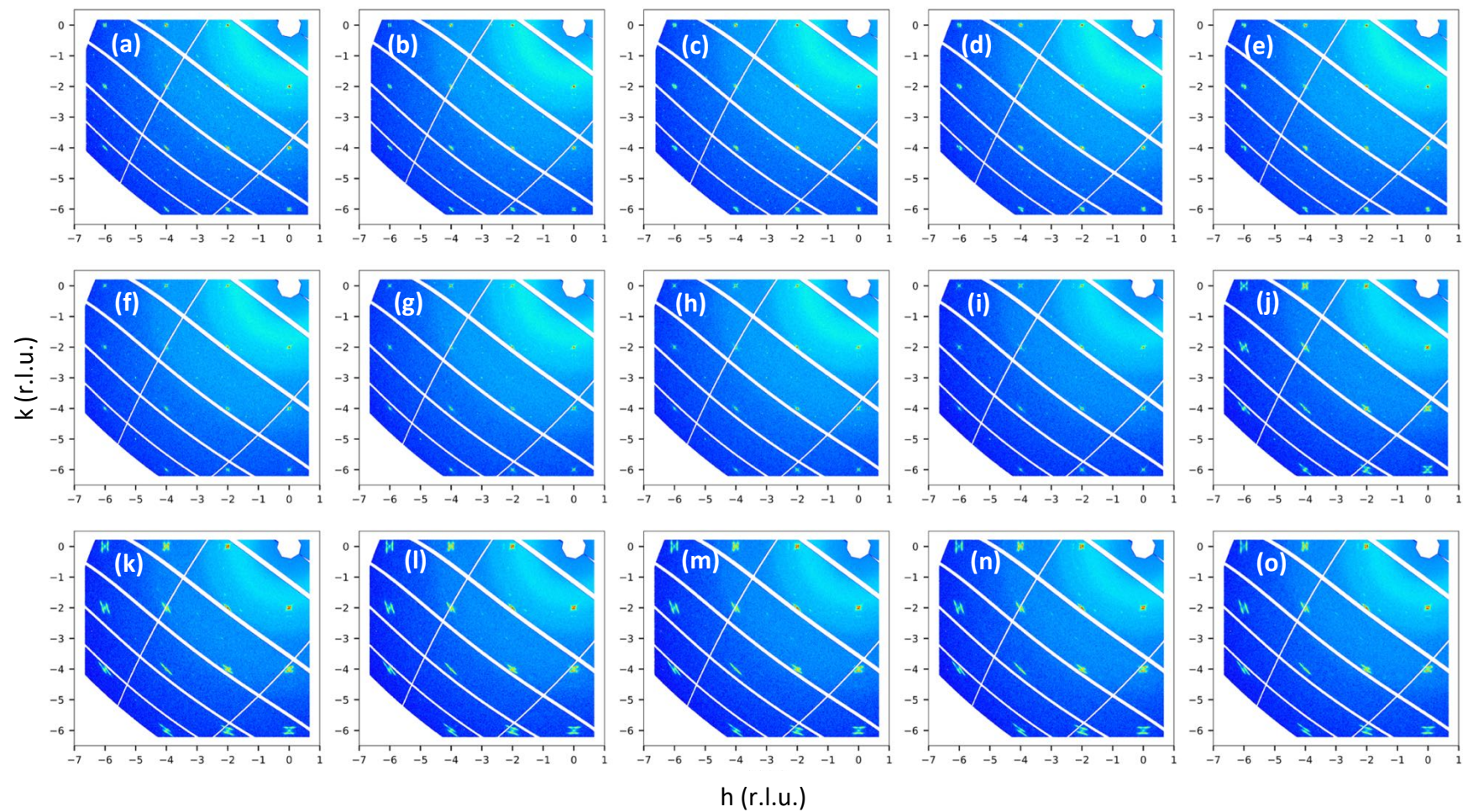


Fig. S4: (HK0)-planes during the electrochemical reduction of $\text{Pr}_2\text{NiO}_{4.225}$ for comparison to the sections reported in Fig 2. The (hk0)-plane also contains an additional complexity related to the formation of epitaxially oriented NiO during the crystal growth and which shows the typical weak reflections as outlined in Fig. S5a-b.

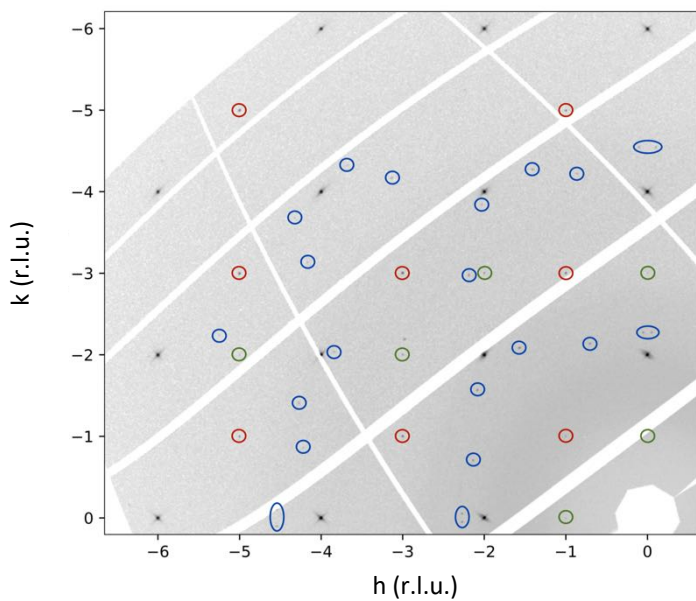


Fig. S5a: reconstructed (hk0)-plane for the $\text{Pr}_2\text{NiO}_{4.10}$ phase, indicating the presence of several superstructure reflections in agreement with the $P4_2/nm$ space group (red), while a few weak reflections marked in green violate the reflection conditions $h + k = 2n$. The blue circles belong to the NiO intergrowth phase, which turns out to be present in all $\text{Pr}_2\text{NiO}_{4+\delta}$ crystals as an unavoidable fraction as described in ref³⁶. The NiO reflections are already present in the starting phase and persist to the fully reduced $\text{Pr}_2\text{NiO}_{4.0}$ phase.

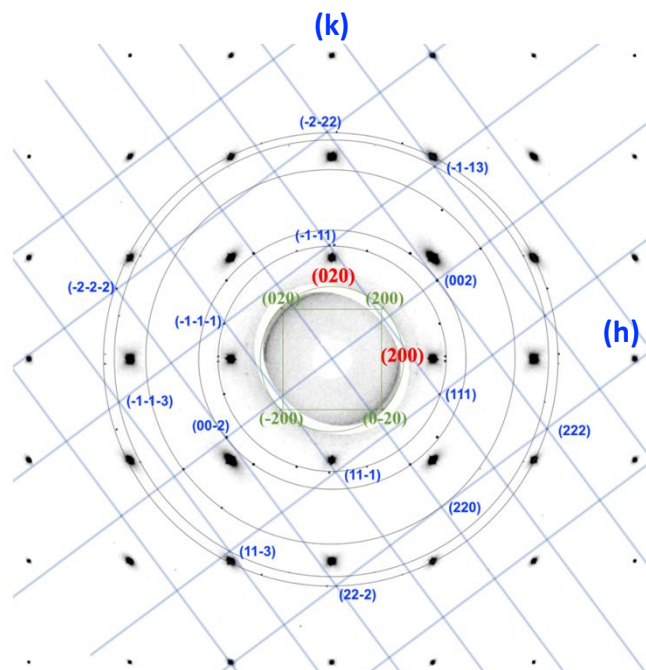


Fig. S5b: Reconstructed (hk0)-plane of $\text{Pr}_2\text{NiO}_{4+\delta}$ obtained from diffraction data on BM01 @ 700°C, (hkl) indexation given in red). [ref 1] This temperature is 335°C above the monoclinic/tetragonal phase transition at 365°C, so no superstructure reflections related to oxygen ordering are observed any more. The additional reflections are related to a small amount of NiO, which is present as an intergrowth phase following NiO segregation as discussed in [ref. 2]. Totally four domains can be identified, which are twinned around [110], indexation is given in blue for one twin domain out of four. Debye-Scherrer lines of the (111), (200), (220), (113) and (222) are outlined to better visualize the equivalence by the same scattering angle, all given in blue. Interestingly there are a few smaller spots with a

higher d-value than the (111)-reflection (green), which correspond by their scattering angle and orientation to Ni_3O_4 , showing a lattice parameter of 8.20Å, which has so far only been described following irradiation damage of NiO as given in [ref 3-4]. Ni_3O_4 is epitaxially grown on $\text{Pr}_2\text{NiO}_{4+\delta}$ with $[100]_{\text{Ni}_3\text{O}_4}$ parallel to the $[110]_{\text{PNO}}$, due to their similar d-values: $d_{(200)}\text{Ni}_3\text{O}_4 = 4.1 \text{ \AA}$, $d_{(220)}\text{PNO} = 3.88\text{\AA}$, resulting into a lattice mismatch of about 5%.

¹ Dutta, R. *et al.* Long-range oxygen ordering linked to topotactic oxygen release in $\text{Pr}_2\text{NiO}_{4+\delta}$ fuel cell cathode material. *Journal of Materials Chemistry A* **8**, 13987-13995, doi:10.1039/D0TA04652C (2020)

² Wahyudi, O. *et al.* Growth of high quality single crystals of strontium doped (Nd,Pr)-nickelates, $\text{Nd}_{2-x}\text{Sr}_x\text{NiO}_{4+\delta}$ and $\text{Pr}_{2-x}\text{Sr}_x\text{NiO}_{4+\delta}$, *Crystengcomm* **17**, 6278-6285, doi:10.1039/c5ce00906e (2015)

³ Buckett, M., & Marks, L. (1988). Formation of a Ni_3O_4 Spinel Phase on the Surface of NiO During Electron Irradiation. *MRS Proceedings*, 129, 521. doi:10.1557/PROC-129-521

⁴ M.I. BUCKETT, *et al.* Electron Irradiation Damage in Oxides, *Ultramicroscopy*, 29 (1989), 217-227

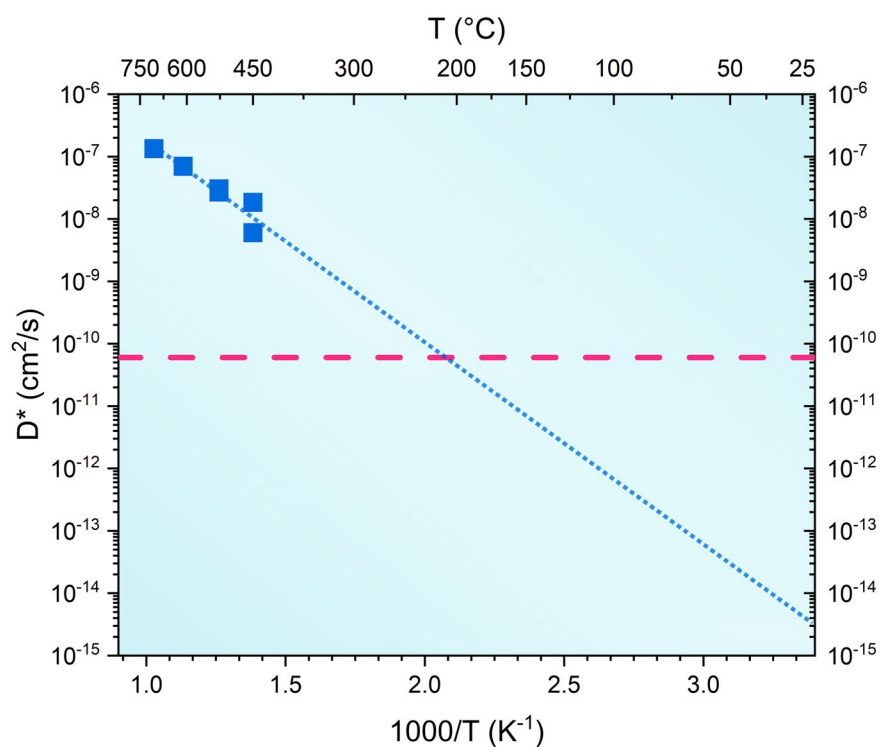


Fig S6: Oxygen diffusion coefficients obtained by the $^{18}\text{O}/^{16}\text{O}$ tracer method on single crystals which can be extrapolated to result at room temperature to yield $D^* \approx 10^{-15} \text{ cm}^2\text{s}^{-1}$, while the corresponding value under electrochemical potential accounts to almost $10^{-10} \text{ cm}^2\text{s}^{-1}$, indicated as a red dashed line. Data taken from ref¹

¹ Bassat, J.-M. *et al.* Anisotropic Oxygen Diffusion Properties in $\text{Pr}_2\text{NiO}_{4+\delta}$ and $\text{Nd}_2\text{NiO}_{4+\delta}$ Single Crystals. *The Journal of Physical Chemistry C* **117**, 26466-26472, doi:10.1021/jp409057k (2013)

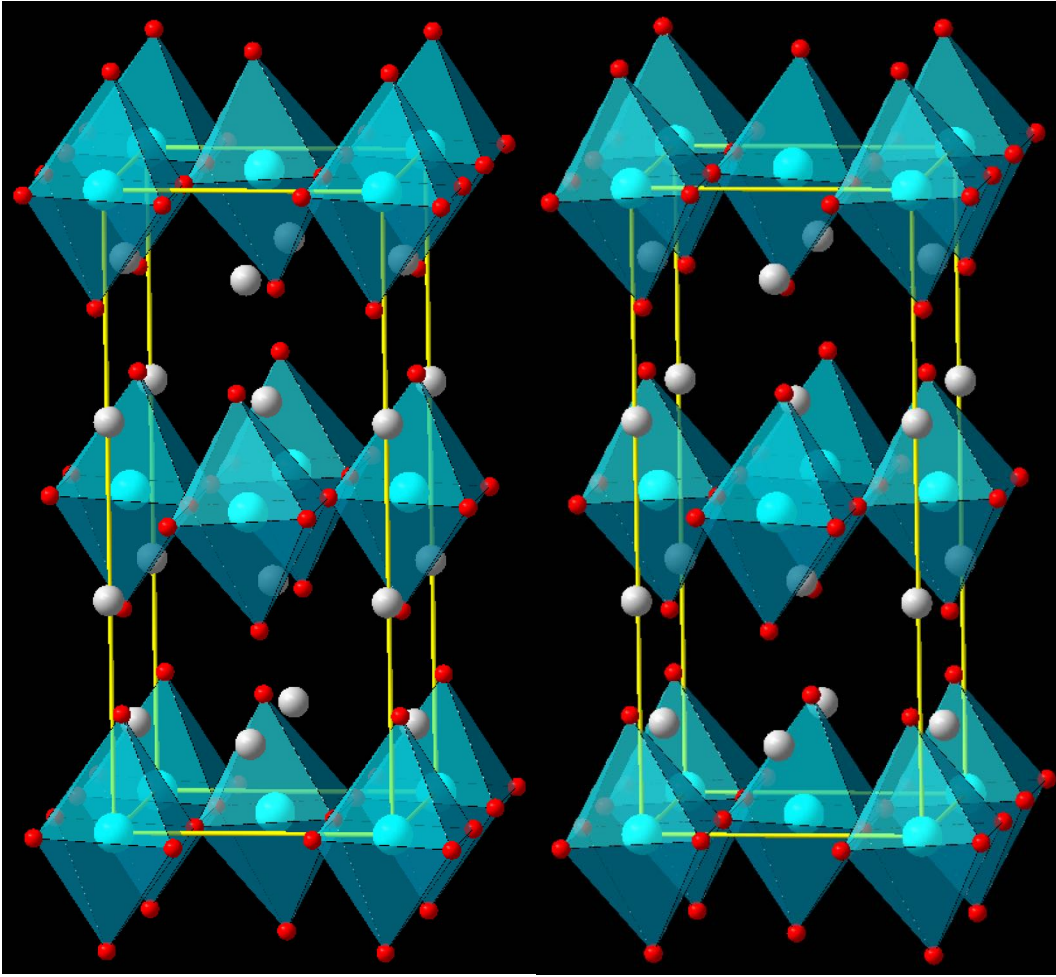


Fig. S7: Schematic presentation of the two anti phase domains in Pr₂NiO_{4.0} showing a different tilt direction for the NiO₆ octahedra.